

Nonideal effect of free electrons on ionization equilibrium and radiative property in dense plasmas

Jiaolong Zeng ^{1,2,*} Yongjun Li,² Yong Hou ² and Jianmin Yuan ^{2,3,†}

¹College of Science, Zhejiang University of Technology, Hangzhou Zhejiang 310023, People's Republic of China

²College of Science, National University of Defense Technology, Changsha Hunan 410073, People's Republic of China

³Graduate School of China Academy of Engineering Physics, Beijing 100193, People's Republic of China



(Received 28 November 2022; accepted 26 February 2023; published 14 March 2023)

The thermodynamic as well as optical properties of strongly coupled plasmas depend crucially on the average degree of ionization and the ionic state composition, which, however, cannot be determined by using the normal Saha equation usually used for the ideal plasmas. Hence, an adequate treatment of the ionization balance and the charge state distribution of strongly coupled plasmas is still a challenge for theory due to the interactions between the electrons and ions and among the electrons themselves. Based on a local density temperature-dependent ionosphere model, the Saha equation approach is extended to the regime of strongly coupled plasmas by taking into account the free-electron-ion interaction, the free-free-electron interaction, the nonuniform free-electron space distribution, and the free-electron quantum partial degeneracy. All the quantities, including the bound orbitals with ionization potential depression, free-electron distribution, and bound and free-electron partition function contributions, are calculated self-consistently in the theoretical formalism. This study shows that the ionization equilibrium is evidently modified by considering the above nonideal characteristics of the free electrons. Our theoretical formalism is validated by the explanation of a recent experimental measurement of the opacity of dense hydrocarbon.

DOI: [10.1103/PhysRevE.107.L033201](https://doi.org/10.1103/PhysRevE.107.L033201)

Dense plasmas occur widely in astrophysical objects such as the stellar interiors and the envelopes and cores of brown dwarfs [1,2], in studies of inertial confinement fusion [3], and in the interaction of intense x-ray lasers with solid-density matter [4]. Accurate description of ionization equilibrium and composition of dense plasmas in local thermodynamic equilibrium (LTE) is of fundamental importance for investigations of the physical properties, including the equation of state and radiative properties. Ongoing efforts have been carried out for several decades to study the ionization equilibrium of dense plasmas; however, both experiments and theories face great challenges. Currently, it cannot be safely asserted that the physics related to the many-body effects encountered have been well understood. Experimentally, the high-energy-density states in dense plasmas are extremely difficult to produce and measure in laboratories. Only a few limited experiments have obtained the average degree of ionization of dense plasmas at several times solid density [5], yet the composition and charge state distributions (CSDs) are still difficult to obtain. The authors of Ref. [5] state that the widely used ionization models need to be modified in order to correctly explain the experimental results of extremely dense states of matter. Recently, a time-resolved experiment was performed via K-shell absorption spectroscopy to measure the ionization states of warm dense aluminum plasma at a close-to-solid density [6]. Although it is possible now to give

multimessenger constraints combined with gravitational-wave and electromagnetic signals of the neutron star equation of state [7], detailed information on the ionization equilibrium and composition of a dense plasma is still ambiguous or even missing.

Theoretically, among the widely used formalisms [8], the most consistent method to investigate the ionization equilibrium of dense plasmas consists of using the physical picture [9], including the activity expansion of the grand canonical partition function [10,11] and the path-integral Monte Carlo method [12]. The first-principles theories, like molecular dynamics simulations using the density functional theory, can also obtain information on the ionization equilibrium, such as average degree of ionization, yet obtaining detailed CSDs and populations of different quantum states are still challenging [13–16]. With increasing the plasma density, however, the physical picture faces well-known mathematical difficulties, and therefore the chemical picture has been used widely instead in practical calculations [17–24]. After several decades of development, the chemical model has now been extended to self-consistently treat the microscopic interinfluence of the plasma-charged particles in the pair correlation approximation [25,26], and the thermodynamic inconsistencies [27–29] can be eliminated using a renormalization theory of plasma particle interactions.

In chemical models, the effects of a dense plasma environment on partition functions and ionization potentials of the ions have usually been considered using different formalisms. However, the effect of nonideal characteristics (NIC) on partition functions of free electrons was not adequately addressed.

*jlzeng@zjut.edu.cn

†jmyuan@gscaep.ac.cn

As we know, the assumption that the free electrons in the plasmas are uniformly distributed in space is in general invalid in dense plasmas. This means that the partition function of the free electrons is different for different charge states. Moreover, recent experimental advances on quantitatively measuring ionization potential depressions (IPDs) of dense plasmas [30–33] motivate further investigations of ionization balance, because IPDs directly enter the Saha equation.

Herein we investigate the plasma nonideal effects on the partition functions of free electrons for different charge states and on the ionization balance of dense plasmas. On the basis of correctly treating the plasma screening effects on the internal partition functions and on the IPDs of each charge state in the plasma, we develop a consistent theoretical formalism to study the nonideal effect of partition functions of free electrons on the ionization balance of dense plasmas.

According to local density Fermi-Dirac distribution of free electrons, in an LTE plasma at a temperature T , the population of charge state $i + 1$ in a phase space $d^3r d^3p$ at a space position of \mathbf{r} and a momentum of \mathbf{p} is determined by

$$\frac{N_{i+1}^{rp}}{N_i} = \frac{Z_{i+1}}{Z_i} \frac{1}{N_e} \frac{2d^3r d^3p}{h^3} e^{-\frac{\phi_i - \Delta\phi_i}{kT}} \frac{1}{e^{\frac{\epsilon + V_i(r)}{kT}} + e^{-\frac{\mu}{kT}}}, \quad (1)$$

where N_i and Z_i are the population density and partition function of charge state i , respectively, N_e the population density of free electrons, μ the chemical potential of the plasma, h the Planck constant, m the rest mass of the electron, k the Boltzmann constant, and $\epsilon = \frac{p^2}{2m}$ the kinetic energy of the free electron. The ionization potential ϕ_i of charge state i refers to that of the isolated ion. The IPD $\Delta\phi_i$ caused by the plasma environment was obtained by a method of temperature-dependent ion-sphere model [34]. The effective potential $V_i(\mathbf{r})$ of the charge state i includes both contributions of the bound electrons and of the plasma screening induced by the environment. The single-electron effective potential, including both bound and free-electron contributions and that being determined self-consistently, represents the effective interaction of a single electron with all other electrons and the nucleus. The static screening potential induced by the charged particles in the plasma is automatically considered by solving the Poisson equation. By integrating over the phase space, one obtains the modified Saha equation,

$$\frac{N_{i+1}N_e}{N_i} = \frac{b_i Z_e Z_{i+1}}{Z_i} e^{-\frac{\phi_i - \Delta\phi_i}{kT}}, \quad (2)$$

where Z_e is the partition function of the uniform electron gas,

$$Z_e = 2 \left(\frac{2\pi m_e kT}{h^2} \right)^{3/2}, \quad (3)$$

and $b_i Z_e$ is the partition function of the free electrons belonging to the charge state i , with b_i being determined by

$$b_i = \frac{1}{\int_0^{R_0} 4\pi r^2 dr} \int_0^{R_0} dr \int_0^\infty d\epsilon \frac{8\pi}{h^3} (2m)^{3/2} r^2 \epsilon^{1/2} \frac{1}{e^{\frac{\epsilon + V_i(r)}{kT}} + e^{-\frac{\mu}{kT}}}, \quad (4)$$

where R_0 denotes the radius of a spherical volume containing the ion of charge state i , which is determined by the matter density $R_0 = \left(\frac{3}{4\pi n_i} \right)^{1/3}$. The central-field approximation is

maintained and thus the potential energy function $V_i(r)$ for the electron is assumed to be spherically symmetrical. This modified Saha equation can be consistently solved with the constraint of particle and charge conservation. In past work [17–24] it was assumed that $V_i(r) = 0$, which means a uniform spatial distribution of the free electrons, then the above equation reduces to the standard Saha equation, where all charge states have the same partition function as expressed by Eq. (3). By including the NIC effects on the free-electron partition functions, the standard Saha equation was generalized to a dense plasma regime.

All physical quantities including the partition functions and ionization potentials required in the modified Saha equation, Eq. (2), are obtained by solving the Dirac equation of each charge state i from the neutral atom to the hydrogenlike ion,

$$[h_i + V_i(r)]\psi(\mathbf{r}) = E_i\psi(\mathbf{r}). \quad (5)$$

The effective single-electron potential of the isolated charge state of i is determined by the flexible atomic code [35]. The plasma screening potential $V_{\text{scr}}(r)$ is assumed to be predominantly contributed by the density function of the free electrons $\rho(r)$ [36–39],

$$V_{\text{scr}}(r) = 4\pi \left[\frac{1}{r} \int_0^r r_1 + \int_r^{R_0} r_1 \rho(r_1) \right] dr_1 - \frac{3}{2} \left[\frac{3}{\pi} \rho(r) \right]^{1/3}. \quad (6)$$

The density function $\rho(r)$ of the free electrons is determined by the ionization balance presented above. As an initial evaluation of the ionization balance, the cutoff of the energy levels in the summation of partition functions and IPDs are determined by the Stewart-Pyatt model [40]. A convergent result is obtained after multiple iterations.

The partition function Z_i of charge state i is calculated over all the available bound quantum states,

$$Z_i = \sum_j g_{j,i} e^{-E_{j,i}/kT}, \quad (7)$$

where $g_{j,i}$ and $E_{j,i}$ are the statistical weights and energies of the quantum state j , respectively, belonging to the charge state i . The ionization potential of the charge state i is determined by the energy difference of the respective ground levels of i and $i + 1$. As the plasma screening potential is put directly into the Hamiltonian of the physical system, the IPD caused by the plasma environment is naturally considered in the calculations. The ionization potential with the inclusion of plasma screening determines the highest possible bound state under the given plasma condition.

In this work we used the formalism [17] to ensure that there is thermodynamic consistency with Maxwell's equations. The NIC effects have been included in the model construction and numerical calculation of the free energy of the whole system, based on self-consistently obtained microstructures. With the same free energy, appropriate changes to thermodynamic quantities such as entropy and pressure are also made in order to ensure that there is thermodynamic consistency.

Previous works used one physical quantity of partition functions of the free electrons in the ionization equilibrium equation [17–24]. In dense plasmas, however, the partition functions of the free electrons for different charge states are

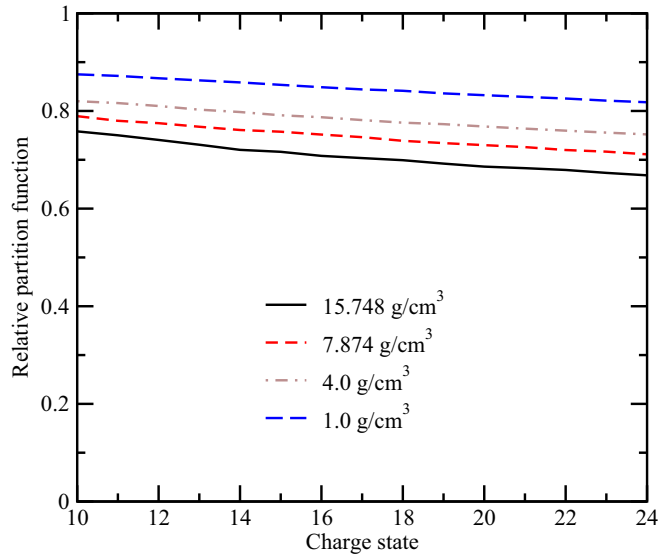


FIG. 1. Relative partition functions (b_i in Eq. (4)) of the free electrons for different charge states in Fe plasmas at a temperature of 200 eV and mass densities of 1.0 g cm⁻³, 4.0 g cm⁻³, 7.874 g cm⁻³, and 15.748 g cm⁻³, respectively. For each plasma condition, the partition functions are relative to that of the uniform electron gas [$Z_e = 2(\frac{2\pi m_e kT}{h^2})^{3/2}$].

different due to different effective potential functions. In Fig. 1 we show the density dependence of the partition functions of the free electrons for different charge states of Fe plasmas at a fixed temperature of 200 eV. The partition functions are relative to the value of $Z_e = 2(\frac{2\pi m_e kT}{h^2})^{3/2}$ of the uniform electron gas. It can be found that the relative partition functions decrease with increasing the mass density of plasma for all charge states. For example, the relative partition functions of Fe¹⁶⁺ decrease from a value of 0.849 at a density of 1.0 g cm⁻³ to 0.708 at a density of 15.748 g cm⁻³. Moreover, at a given plasma condition of definite temperature and density, the relative partition functions decrease with increasing ionization state. We suggest that part of the free electrons move with the ions, and the higher the ionization state, the more the free electrons move along with the ions. The free electrons of this part moving along with the ions distinguish themselves from the truly bound electrons belonging to the ions, yet they also behave differently from the other free electrons, which can freely move in the plasma [41].

Figure 2 shows the temperature dependence of relative partition functions of the free electrons for different charge states of Fe plasmas at a mass density of 7.874 g cm⁻³. Obviously, the relative partition functions increase with increasing the plasma temperature for all ionization states. From Figs. 1 and 2, one can reasonably deduce that the relative partition functions of the free electrons tend towards unity with decreasing plasma density or increasing plasma temperature.

The effect of NIC on the partition functions of the free electrons will definitely affect the ionization balance. Its effect on the charge state distributions is shown in Fig. 3 at different mass densities of 1.0, 7.874, and 15.748 g cm⁻³ and temperatures of 100, 200, 300, 600, and 1000 eV, respectively. With this effect included, the CSDs move to lower ionization states.

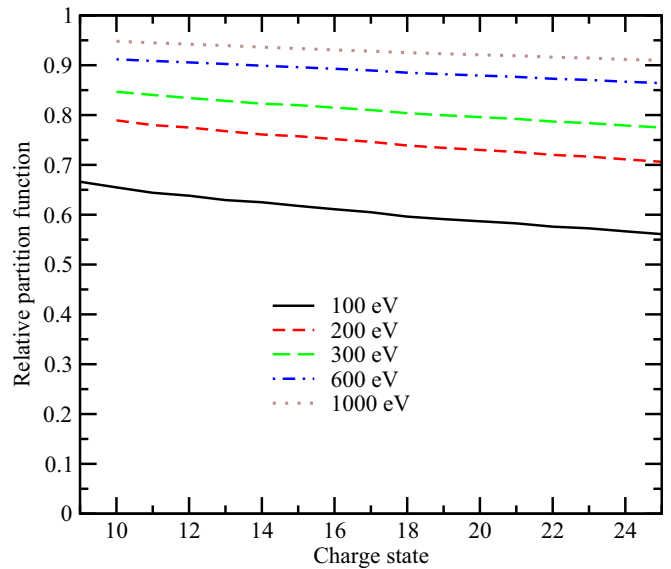


FIG. 2. Relative partition functions (b_i in Eq. (4)) of the free electrons for different charge states in Fe plasmas at a mass density of 7.874 g cm⁻³ and temperatures of 100 eV, 200 eV, 300 eV, 600 eV, and 1000 eV, respectively. For each plasma condition, the partition functions are relative to those of the uniform electron gas [$Z_e = 2(\frac{2\pi m_e kT}{h^2})^{3/2}$].

In general, the NIC show a more pronounced effect on the CSDs with increasing plasma density and decreasing plasma temperature, which is in accordance with the NIC effect on the partition functions of the free electrons. At a density of 1.0 g cm⁻³, the difference between the CSDs with or without considering the NIC effect is becoming smaller with increasing the plasma temperature, and such difference of the CSDs becomes too small to be observable at a temperature above 600 eV. With increasing the plasma density, however, the onset plasma temperature becomes higher, at which the CSDs show nearly equivalent values with or without considering the effect of NIC on the partition functions of the free electrons.

At a temperature of 200 eV and densities of 7.874 and 15.748 g cm⁻³, a new phenomenon of two-peak structure shows up in the CSDs by either considering the NIC effect or not, which is completely different from the single-peak distribution of CSDs at other plasma conditions. The population fractions of Fe¹⁴⁺ and Fe¹⁶⁺ are larger than that of Fe¹⁵⁺, resulting in the two-peak values of populations in Fe¹⁴⁺ and Fe¹⁶⁺. At these plasma conditions, large IPDs are predicted due to the plasma screening [34,38,39], and thus the ionization potentials of screened Fe¹⁴⁺ (46.7 eV at a density of 15.748 g cm⁻³) and Fe¹⁵⁺ (51.4 eV at a density of 15.748 g cm⁻³) are much smaller than the corresponding values of isolated Fe¹⁴⁺ ion (456.2 eV [42]) and Fe¹⁵⁺ ion (489.3 eV [42]). However, the screened Ne-like Fe¹⁶⁺ (775.8 eV at a density of 15.748 g cm⁻³) still has a much larger ionization potential than Fe¹⁴⁺ and Fe¹⁵⁺. As a result, the population of Fe¹⁵⁺ is decreased compared with that of Fe¹⁴⁺ because the partition function of Fe¹⁵⁺ is much smaller than that of Fe¹⁴⁺. The two-peak CSDs should be a common phenomenon in dense plasmas when the plasma density is high enough that the ionization potentials of a number of charge states are relatively close

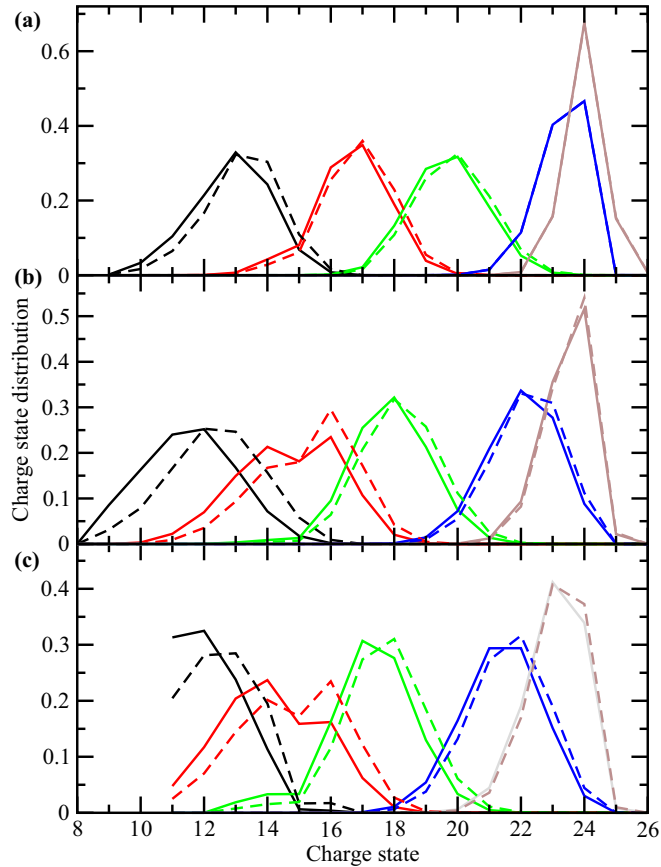


FIG. 3. Comparison of charge state distribution of Fe plasmas with (solid lines) and without (dashed lines) considering the effect of NIC of free electrons at mass densities of (a) 1.0 g cm^{-3} , (b) 7.874 g cm^{-3} , and (c) 15.748 g cm^{-3} and at temperatures of 100 eV (solid and dashed black lines), 200 eV (solid and dashed red lines), 300 eV (solid and dashed green lines), 600 eV (solid and dashed blue lines), and 1000 eV (solid and dashed brown lines).

to each other due to plasma screening. It is also obvious that pressure ionization dominates the ionization equilibrium at a density of 15.748 g cm^{-3} and a temperature of 100 eV. Pressure ionization is of fundamental interest in both condensed matter physics and plasma physics in providing equations of state for astrophysics and inertial confinement fusion research. However, large discrepancies are found between different chemical models and the first-principles simulations [43–45], and therefore, it still remains a controversial problem.

The phenomenon of double-peak structure for CSDs can be found in both light and heavy elements at different regimes of plasma density and temperature. This phenomenon happens in a plasma regime where both pressure ionization and thermal ionization play a role in the determination of ionization balance. If the plasma density is so low that pressure ionization cannot happen, then it cannot be observed. However, if pressure ionization dominates over thermal ionization, it is still difficult to occur. When pressure ionization happens and then thermal ionization starts exceeding pressure ionization, this phenomenon naturally emerges. Thus it can be found in both light and heavy elements. It can be shown in a wider regime of density and temperature for heavier elements than

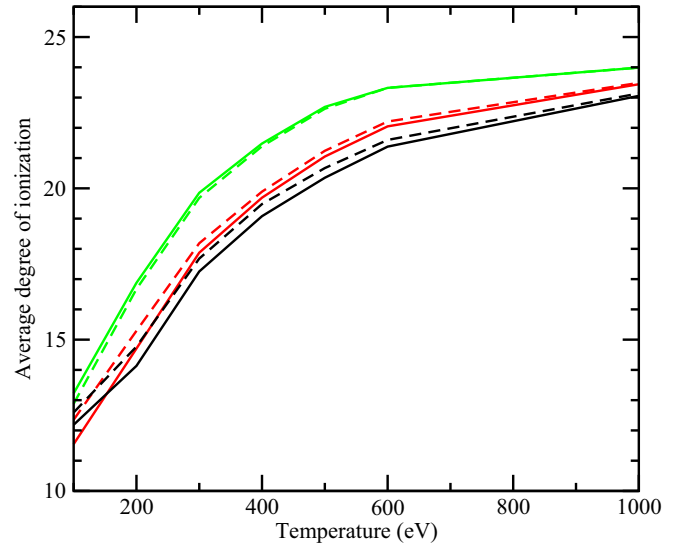


FIG. 4. Comparison of average degree of ionization of Fe plasmas with (solid black and colored lines) and without (dashed black and colored lines) considering the effect of NIC of free electrons as a function of plasma temperature at mass densities of 1.0 g cm^{-3} (green lines), 7.874 g cm^{-3} (red lines), and 15.748 g cm^{-3} (black lines).

for lighter elements, because of the greater number of charge states, electronic subshells, and closer ionization potentials of the neighboring charged ions. The IPD is quite essential for the appearance of the double peak in CSDs, because the IPD effect is stronger for higher charged ions and makes the actual ionization potential of neighboring charged ions closer to each other compared to the corresponding isolated ions. If the IPD caused by plasma screening is not considered in the ionization balance equation, the double-peak structure is much more difficult to be observed in the CSDs. Thus the opacity is in general decreased, and the pressure in the equation of state is in general increased if we consider the IPD in the ionization balance. This conclusion is also true if the nonideality effect in free-electron partition functions is not considered while other NIC effects discussed in this work are included.

The NIC effect on the average degree of ionization of Fe plasmas is shown in Fig. 4 as a function of plasma temperature. It can be easily seen that this effect becomes larger in general with increasing the plasma density. However, if pressure ionization played a more important role than thermal ionization, then the above conclusion may not be right. For example, the NIC effect on the average degree of ionization is smaller at 15.748 g cm^{-3} than that at 7.874 g cm^{-3} at a lower plasma temperature (below $\sim 180 \text{ eV}$). At the experimental condition of several times solid density and an average temperature of $86 \pm 20 \text{ eV}$ [5], the pressure ionization plays a dominant role, and therefore the NIC effect on the average degree of ionization should be relatively small.

As is well known, the ionization balance of plasma affects its physical properties such as the opacity [46–56] and the equation of state, and thus constitutes the basis for further investigations on the dense plasmas. Here we interpret the opacity measurement carried out by Kritcher *et al.* [1] using the developed theoretical formalism. This experiment reports

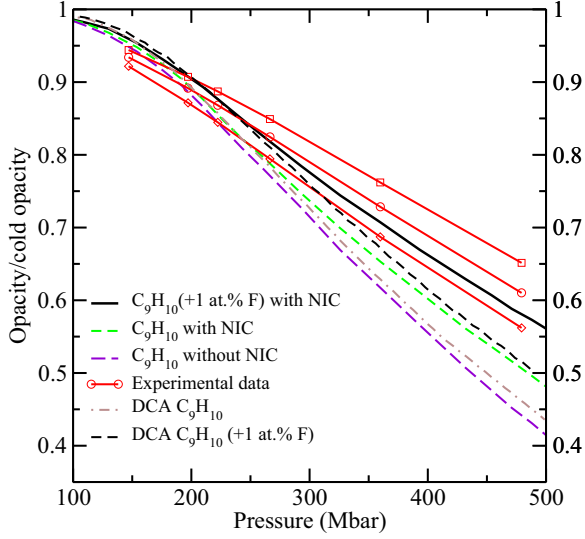


FIG. 5. Opacity of dense C_9H_{10} at a photon energy of 9 keV with and without considering the NIC effect. The plasma conditions are determined at the shock front along the shock Hugoniot (central red line) measured by Kritcher *et al.* [1]. Another two red lines correspond to uncertainty contours in the measurement. We also give the theoretical results of the normalized opacity with and without 1 at % F (black line). Comparisons are made with the experimental measurement and theoretical results through detailed configuration accounting (DCA) [1].

the equation of state along the principal shock Hugoniot of hydrocarbon with pressures ranging from 100 million to 450 million atmospheres. To interpret the experimental measurements in this high-energy-density regime, they simultaneously measured the opacity of the dense hydrocarbon. Figure 5 shows the opacity of the dense C_9H_{10} at the shock front normalized to the cold material opacity as a function of shock-front pressure at a photon energy of 9 keV. The densities and temperatures of C_9H_{10} obtained from very recent theoretical work [13] and a few other cases are given in Table I. Our predicted relative opacity is compared with the experimental (central red line) [1] and other theoretical results of non-LTE modeling using a detailed configuration accounting (DCA) method [57]. The experimental uncertainty contours of $\pm\sigma$ in the measurement were given by another two red lines. As the experimental samples were mixed with uniform trace amounts of fluorine (1 at %), we also give the theoretical results of the normalized opacity with 1 at % F (black line).

TABLE I. A few data points of densities (g/cm^3), temperatures (eV), and pressures (Mbar) of C_9H_{10} along the principal shock Hugoniot in the experiment [1]. The data are obtained from the first-principles calculations of Ref. [13].

| Density | Temperature | Pressure |
|---------|-------------|----------|
| 4.557 | 72.05 | 161.7 |
| 4.774 | 102.09 | 255.3 |
| 4.937 | 163.97 | 467.6 |
| 4.774 | 308.83 | 946.8 |

From Fig. 5, only when we have included the NIC effect (black line with 1 at % F) can we reasonably explain the measured opacity [1]. Without considering the NIC effect, either the non-LTE DCA modeling [57] or our LTE detailed level accounting calculations predict a much lower opacity at higher pressures, irrespective of whether including the contribution of trace element of fluorine or not. Then we point out that such a reasonable explanation of the experimental data is purely a result of the correct treatment of the ionization balance. As we know, the opacity is contributed by bound-bound, bound-free, free-free, and scattering processes [58]. At the above plasma conditions, the dominant contribution originates from the bound-free process, which is determined by the populations and photoionization cross sections,

$$\kappa_{bf}(h\nu) = \frac{1}{\rho} \sum_i \sum_l N_{il} \sigma_{il}(h\nu), \quad (8)$$

where $h\nu$ denotes the photon energy, ρ denotes the mass density of plasma, N_{il} denotes the population of level l , of charge state i , and σ_{il} denotes the photoionization cross section. A photon energy of 9 keV is well above the ionization potentials of isolated and screened C^{4+} and C^{5+} , and thus the plasma screening effect on the photoionization cross sections is small at such a high photon energy. As a result, the different theoretical results are predominantly due to a distinction in the different treatment of the ionization balance. Measuring the opacity at a high photon energy (as in the experiment [1]) provides us with an alternative method of measuring the ionization equilibrium of dense plasmas because a direct experiment is still challenging. We also note that at the recent experimental conditions [59,60], the plasma density is still small and hence the NIC effect should be small as well. The NIC effect should not be the dominant reason for the large discrepancy between experiment and theory. There should exist other novel mechanisms in the calculation of opacity [61].

In summary, we have investigated the effects of a dense plasma environment on the partition functions of free electrons and on the ionization equilibrium. A completely consistent theoretical formalism is developed to treat the partition functions of ions and free electrons and ionization potentials of different ionization states through introducing the plasma screening potential. By removing the widely used assumption of uniform electron gas of the free electrons, we obtain a modified Saha ionization equilibrium equation. In general, at a given plasma temperature, the relative partition functions of free electrons decrease with increasing the plasma density, and at a given plasma density, they increase with increasing the plasma temperature. Including the effect of nonideal distribution of free electrons, the predicted charge state distributions move towards lower ionization states in general and hence the average degree of ionization becomes lower. At the limit of low plasma density and high temperature, our theory naturally returns to the usually widely used ionization equilibrium equation without considering the effect of nonideal characteristics of free electrons. We note that the two-peak structure in the charge state distributions and pressure ionization should be common phenomena in dense plasmas, especially for medium- and high-Z materials. Our

theory successfully explains the recent experimental measurement of the opacity of dense C_9H_{10} at a photon energy of 9 keV, which validates the present theoretical formalism.

This work was supported by the National Natural Science Foundation of China under Grants No. 12174343, No. 12274384, and No. 11974424.

-
- [1] A. L. Kritcher, D. C. Swift, T. Döppner, B. Bachmann, L. X. Benedict, G. W. Collins, J. L. DuBois, F. Elsner, G. Fontaine, J. A. Gaffney *et al.*, A measurement of the equation of state of carbon envelopes of white dwarfs, *Nature (London)* **584**, 51 (2020).
- [2] N. Giammichele, S. Charpinet, G. Fontaine, E. M. Green, V. Van Grootel, W. Zong, and M. A. Dupret, A large oxygen-dominated core from the seismic cartography of a pulsating white dwarf, *Nature (London)* **554**, 73 (2018).
- [3] O. A. Hurricane, D. A. Callahan, D. T. Casey, P. M. Celliers, C. Cerjan, E. L. Dewald, T. R. Dittrich, T. Döppner, D. E. Hinkel, L. F. Berzak Hopkins *et al.*, Fuel gain exceeding unity in an inertially confined fusion implosion, *Nature (London)* **506**, 343 (2014).
- [4] E. A. Seddon, J. A. Clarke, D. J. Dunning, C. Masciovecchio, C. J. Milne, F. Parmigiani, D. Rugg, J. C. H. Spence, N. R. Thompson, K. Ueda, S. M. Vinko, J. S. Wark, and W. Wurth, Short-wavelength free-electron laser sources and science: A review, *Rep. Prog. Phys.* **80**, 115901 (2017).
- [5] D. Kraus, D. A. Chapman, A. L. Kritcher, R. A. Baggott, B. Bachmann, G. W. Collins, S. H. Glenzer, J. A. Hawreliak, D. H. Kalantar, O. L. Landen, T. Ma, S. Le Pape, J. Nilsen, D. C. Swift, P. Neumayer, R. W. Falcone, D. O. Gericke, and T. Döppner, X-ray scattering measurements on imploding CH spheres at the National Ignition Facility, *Phys. Rev. E* **94**, 011202(R) (2016).
- [6] M. Z. Mo, Z. Chen, S. Fourmaux, A. Saraf, S. Kerr, K. Otani, R. Masoud, J. C. Kieffer, Y. Tsui, A. Ng, and R. Fedosejevs, Measurements of ionization states in warm dense aluminum with betatron radiation, *Phys. Rev. E* **95**, 053208 (2017).
- [7] T. Dietrich, M. W. Coughlin, P. T. H. Pang, M. Bulla, J. Heinzl, L. Issa, I. Tews, and S. Antier, Multimessenger constraints on the neutron-star equation of state and the Hubble constant, *Science* **370**, 1450 (2020).
- [8] F. J. Rogers, Ionization equilibrium and equation of state in strongly coupled plasmas, *Phys. Plasmas* **7**, 51 (2000).
- [9] W. Ebeling, W. D. Kraeft, and D. Kremp, *Theory of Bound States and Ionization Equilibrium* (Akademie-Verlag, Berlin, 1976).
- [10] F. J. Rogers, F. J. Swenson, and C. A. Iglesias, OPAL equation-of-state tables for astrophysical applications, *Astrophys. J.* **456**, 902 (1996).
- [11] F. J. Rogers and D. A. Young, Validation of the activity expansion method with ultrahigh pressure shock equations of state, *Phys. Rev. E* **56**, 5876 (1997).
- [12] W. R. Magro, D. M. Ceperley, C. Pierleoni, and B. Bernu, Molecular Dissociation in Hot, Dense Hydrogen, *Phys. Rev. Lett.* **76**, 1240 (1996).
- [13] X. Liu, X. Zhang, C. Gao, S. Zhang, C. Wang, D. Li, P. Zhang, W. Kang, W. Zhang, and X. T. He, Equations of state of poly- α -methylstyrene and polystyrene: First-principles calculations versus precision measurements, *Phys. Rev. B* **103**, 174111 (2021).
- [14] J. Dai, Y. Hou, and J. Yuan, Unified First Principles Description from Warm Dense Matter to Ideal Ionized Gas Plasma: Electron-Ion Collisions Induced Friction, *Phys. Rev. Lett.* **104**, 245001 (2010).
- [15] T. J. Lenosky, J. D. Kress, and L. A. Collins, Molecular-dynamics modeling of the Hugoniot of shocked liquid deuterium, *Phys. Rev. B* **56**, 5164 (1997).
- [16] F. Perrot and M. W. C. Dharma-Wardana, Equation of state and transport properties of an interacting multispecies plasma: Application to a multiply ionized Al plasma, *Phys. Rev. E* **52**, 5352 (1995).
- [17] D. Mihalas, W. Däppen, and D. Hummer, The equation of state for stellar envelopes. II. Algorithm and selected results, *Astrophys. J.* **331**, 815 (1988).
- [18] D. Saumon and G. Chabrier, Fluid hydrogen at high density: Pressure dissociation, *Phys. Rev. A* **44**, 5122 (1991).
- [19] A. Y. Potekhin, G. Massacrier, and G. Chabrier, Equation of state for partially ionized carbon at high temperatures, *Phys. Rev. E* **72**, 046402 (2005).
- [20] M. R. Zaghoul, Integrability criterion for lowering of ionization potentials and formulation of the solution of the inverse problem of constructing consistent thermodynamic functions of nonideal plasmas, *Phys. Rev. E* **79**, 016410 (2009).
- [21] Y. V. Arkipov, F. B. Baimbetov, and A. E. Davletov, Ionization equilibrium and equation of state of partially ionized hydrogen plasmas: Pseudopotential approach in chemical picture, *Phys. Plasmas* **12**, 082701 (2005).
- [22] K. Wang, Z. Shi, Y. Shi, J. Bai, J. Wu, and S. Jia, The equation of state and ionization equilibrium of dense aluminum plasma with conductivity verification, *Phys. Plasmas* **22**, 062709 (2015).
- [23] T. S. Ramazanov, M. T. Gabdullin, K. N. Dzhumagulova, and R. Redmer, Ionization equilibrium and composition of a dense partially ionized metal plasma, *Contrib. Plasma Phys.* **51**, 391 (2011).
- [24] I. Shimamura and T. Fujimoto, State densities and ionization equilibrium of atoms in dense plasmas, *Phys. Rev. A* **42**, 2346 (1990).
- [25] Yu. V. Arkipov, F. B. Baimbetov, and A. E. Davletov, Self-consistent chemical model of partially ionized plasmas, *Phys. Rev. E* **83**, 016405 (2011).
- [26] A. E. Davletov, F. Kurbanov, and Y. S. Mukhametkarimov, Influence of dust particles on ionization equilibrium in partially ionized plasmas, *Phys. Rev. E* **101**, 063203 (2020).
- [27] M. Sweeney, Thermodynamic inconsistency of the modified Saha equation at high pressures, *Astrophys. J.* **220**, 335 (1978).
- [28] K. H. Böhm, Pressure ionization in white-dwarf convection zones, *Astrophys. J.* **162**, 919 (1970).
- [29] W. C. Straka, A determination of the lower mass limit for the main sequence, *Astrophys. J.* **165**, 106 (1971).
- [30] O. Ciricosta, S. M. Vinko, H. K. Chung, B. I. Cho, C. R. D. Brown, T. Burian, J. Chalupsky, K. Engelhorn, R. W. Falcone, C. Graves, V. Hajkova, A. Higginbotham, L. Juha, J. Krzywinski, H. J. Lee, M. Messerschmidt, C. D. Murphy, Y. Ping, D. S. Rackstraw, A. Scherz *et al.*, Direct Measurements of the Ionization Potential Depression in a Dense Plasma, *Phys. Rev. Lett.* **109**, 065002 (2012).

- [31] D. J. Hoarty, P. Allan, S. F. James, C. R. D. Brown, L. M. R. Hobbs, M. P. Hill, J. W. O. Harris, J. Morton, M. G. Brookes, R. Shepherd, J. Dunn, H. Chen, E. Von Marley, P. Beiersdorfer, H. K. Chung, R. W. Lee, G. Brown, and J. Emig, Observations of the Effect of Ionization-Potential Depression in Hot Dense Plasma, *Phys. Rev. Lett.* **110**, 265003 (2013).
- [32] O. Ciricosta, S. M. Vinko, B. Barbreil, D. S. Rackstraw, T. R. Preston, T. Burián, J. Chalupský, B. I. Cho, H. -K. Chung, G. L. Dakovski *et al.*, Measurements of continuum lowering in solid-density plasmas created from elements and compounds, *Nat. Commun.* **7**, 11713 (2016).
- [33] L. B. Fletcher, A. L. Kritcher, A. Pak, T. Ma, T. Döppner, C. Fortmann, L. Divol, O. S. Jones, O. L. Landen, H. A. Scott, J. Vorberger, D. A. Chapman, D. O. Gericke, B. A. Mattern, G. T. Seidler, G. Gregori, R. W. Falcone, and S. H. Glenzer, Observations of Continuum Depression in Warm Dense Matter with X-Ray Thomson Scattering, *Phys. Rev. Lett.* **112**, 145004 (2014).
- [34] J. L. Zeng, C. Ye, Y. J. Li, and J. M. Yuan, Ionization potential depression in dense iron plasmas near solid density, *Results Phys.* **40**, 105836 (2022).
- [35] M. F. Gu, The flexible atomic code, *Can. J. Phys.* **86**, 675 (2008).
- [36] S.-K. Son, R. Thiele, Z. Jurek, B. Ziąja, and R. Santra, Quantum-Mechanical Calculation of Ionization-Potential Lowering in Dense Plasmas, *Phys. Rev. X* **4**, 031004 (2014).
- [37] Y. Q. Li, J. H. Wu, Y. Hou, and J. M. Yuan, Influence of hot and dense plasmas on energy levels and oscillator strengths of ions: Beryllium-like ions for $Z=26-36$, *J. Phys. B: At. Mol. Opt. Phys.* **41**, 145002 (2008).
- [38] J. L. Zeng, Y. J. Li, C. Gao, and J. M. Yuan, Screening potential and continuum lowering in a dense plasma under solar-interior conditions, *Astron. Astrophys.* **634**, A117 (2020).
- [39] J. L. Zeng, Y. J. Li, Y. Hou, C. Gao, and J. M. Yuan, Ionization potential depression and ionization balance in dense carbon plasma under solar and stellar interior conditions, *Astron. Astrophys.* **644**, A92 (2020).
- [40] J. C. Stewart and K. D. Pyatt, Jr., Lowering of ionization potentials in plasmas, *Astrophys. J.* **144**, 1203 (1966).
- [41] Y. Hou and J. Yuan, Alternative ion-ion pair-potential applied to molecular dynamics simulations of hot and dense plasmas: Al and Fe as example, *Phys. Rev. E* **79**, 016402 (2009).
- [42] A. Kramida, Y. Ralchenko, J. Reader, and NIST ASD Team (2022), NIST Atomic Spectra Database (ver. 5.9), Online, <https://physics.nist.gov/asd> [2022, May 23], National Institute of Standards and Technology, Gaithersburg, MD, DOI: <https://dx.doi.org/10.18434/T4W30F>.
- [43] Q. Li, H. Liu, G. Zhang, Y. Zhao, G. Lu, M. Tian, and H. Song, The thermodynamical instability induced by pressure ionization in fluid helium, *Phys. Plasmas* **23**, 112709 (2016).
- [44] D. Beule, W. Ebeling, A. Förster, H. Juránek, S. Nagel, R. Redmer, and G. Röpke, Equation of state for hydrogen below 10000 K: From the fluid to the plasma, *Phys. Rev. B* **59**, 14177 (1999).
- [45] M. A. Morales, C. Pierleoni, E. Schwegler, and D. M. Ceperley, Evidence for a first-order liquid-liquid transition in high-pressure hydrogen from ab initio simulations, *Proc. Natl. Acad. Sci. USA* **107**, 12799 (2010).
- [46] C. A. Iglesias and F. J. Rogers, Updated OPAL opacities, *Astrophys. J.* **464**, 943 (1996).
- [47] M. J. Seaton, Y. Yan, D. Mihalas, and A. K. Pradhan, Opacities for stellar envelopes, *Mon. Not. R. Astron. Soc.* **266**, 805 (1994).
- [48] S. B. Hansen, J. Bauche, C. Bauche-Arnoult, and M. F. Gu, Hybrid atomic models for spectroscopic plasma diagnostics, *High Energy Density Phys.* **3**, 109 (2007).
- [49] Q. Porcherot, J. C. Pain, F. Gilleron, and T. A. Blenski, Consistent approach for mixed detailed and statistical calculation of opacities in hot plasmas, *High Energy Density Phys.* **7**, 234 (2011).
- [50] C. Blancard, P. Cossé, and G. Faussurier, Solar mixture opacity calculations using detailed configuration and level accounting treatments, *Astrophys. J.* **745**, 10 (2012).
- [51] J. C. Pain and F. Gilleron, Accounting for highly excited states in detailed opacity calculations, *High Energy Density Phys.* **15**, 30 (2015).
- [52] C. J. Fontes, C. L. Fryer, A. L. Hungerford, P. Hakel, J. Colgan, D. P. Kilcrease, and M. E. Sherrill, Relativistic opacities for astrophysical applications, *High Energy Density Phys.* **16**, 53 (2015).
- [53] R. M. More, S. B. Hansen, and T. Nagayama, Opacity from two-photon processes, *High Energy Density Phys.* **24**, 44 (2017).
- [54] M. Krief, Y. Kurzweil, A. Feigel, and D. Gazit, The effect of ionic correlations on radiative properties in the solar interior and terrestrial experiments, *Astrophys. J.* **856**, 135 (2018).
- [55] J. Colgan, D. P. Kilcrease, N. H. Magee, M. E. Sherrill, J. Abdallah Jr., P. Hakel, C. J. Fontes, J. A. Guzik, and K. A. Mussack, A new generation of Los Alamos opacity tables, *Astrophys. J.* **817**, 116 (2016).
- [56] C. A. Iglesias and S. B. Hansen, Fe XVII opacity at solar interior conditions, *Astrophys. J.* **835**, 284 (2017).
- [57] H. A. Scott and S. B. Hansen, Advances in NLTE modeling for integrated simulations, *High Energy Density Phys.* **6**, 39 (2010).
- [58] C. Gao, J. L. Zeng, Y. Q. Li, F. T. Jin, and J. M. Yuan, Versatile code DLAYZ for investigating population kinetics and radiative properties of plasmas in non-local thermodynamic equilibrium, *High Energy Density Phys.* **9**, 583 (2013).
- [59] J. E. Bailey, T. Nagayama, G. P. Loisel, G. A. Rochau, C. Blancard, J. Colgan, Ph. Cosse, G. Faussurier, C. J. Fontes, F. Gilleron *et al.*, A higher-than-predicted measurement of iron opacity at solar interior temperatures, *Nature (London)* **517**, 56 (2015).
- [60] T. Nagayama, J. E. Bailey, G. P. Loisel, G. S. Dunham, G. A. Rochau, C. Blancard, J. Colgan, P. Cossé, G. Faussurier, C. J. Fontes, F. Gilleron, S. B. Hansen, C. A. Iglesias, I. E. Golovkin, D. P. Kilcrease, J. J. MacFarlane, R. C. Mancini, R. M. More, C. Orban, J.-C. Pain *et al.*, Systematic Study of L-Shell Opacity at Stellar Interior Temperatures, *Phys. Rev. Lett.* **122**, 235001 (2019).
- [61] J. L. Zeng, C. Gao, P. F. Liu, Y. J. Li, C. S. Meng, Y. Hou, D. D. Kang, and J. M. Yuan, Electron localization enhanced photon absorption for the missing opacity in solar interior, *Sci. China Phys., Mech. Astron.* **65**, 233011 (2022).